

Research Paper

Evaluation of dust extinction and vertical profiles simulated by WRF-Chem with CALIPSO and AERONET over North Africa

Abdoul Aziz Saidou Chaibou^a, Xiaoyan Ma^{a,*}, Kanike Raghavendra Kumar^b, Hailing Jia^a,
Yaoguo Tang^a, Tong Sha^a

^a Collaborative Innovation Centre on Forecast and Evaluation of Meteorological Disasters, Key Laboratory of Meteorological Disaster, Ministry of Education (KLME), International Joint Laboratory on Climate and Environment Change (ILCEC), Key Laboratory for Aerosol-Cloud-Precipitation of China Meteorological Administration, School of Atmospheric Physics, Nanjing University of Information Science and Technology, Nanjing, 210044, Jiangsu, China

^b Department of Physics, School of Sciences and Humanities, Koneru Lakshmaiah Education Foundation, K. L. University, Vaddeswaram, 522502, Guntur, Andhra Pradesh, India



ARTICLE INFO

Keywords:

Dust aerosols
CALIOP
Sahara

ABSTRACT

In this study, the Weather Research and Forecasting model with Chemistry (WRF-Chem) is applied to compare the simulated dust content and extinction coefficients from the Goddard Chemistry Aerosol Radiation and Transport (GOCART), the Air Force Weather Agency (AFWA) and University of Cologne (UoC) dust emission scheme available in WRF-Chem. The observations made by the Aerosol Robotic Network (AERONET) and Cloud-Aerosol Lidar and Infrared Pathfinder Satellite Observations (CALIPSO) are used to assess the model performance during the summer of 2006 over northern Africa. The results highlight that all the three schemes reproduce broadly the observed spatiotemporal distribution of dust content and extinction profile over northern Africa. However, differences exist in extent and intensity between the three emissions schemes and observations. All the three dust emission schemes reproduce the daily variation of the major dust events observed from the AERONET stations over northern Africa but failed to capture correctly the spatial distribution of the maximum zones of observed dust content by CALIOP. It is found that the simulated dust extinction profiles overestimate broadly the observation from CALIPSO in terms of vertical extent and magnitude over northern Africa. Our results reveal significant differences between the three schemes (GOCART, AFWA, and UoC). These differences between the schemes could be related to the calculation of the threshold wind speed in each scheme, which indicating the necessity to continue improving these dust emission schemes in the WRF-Chem model to better reduce uncertainties in the representation of dust plumes.

1. Introduction

Mineral dust aerosols are mainly emitted by wind erosion in arid and semi-arid regions of the World. The Sahara Desert and semi-arid region of the Sahel, are considered as a main source of mineral dust globally (Goudie and Middleton, 2001; Prospero et al., 2002; Barkan et al., 2004; Engelstaedter et al., 2006). During desert storms, a large quantity of dust is lifted from the earth's surface and injected into the atmosphere to great distances at a typical height between four to 5 km (Prospero, 1996; Prospero and Mayol-Bracero, 2013; Teixeira et al., 2016). In northern Africa, dust emissions occur regularly during the year, and are mainly controlled by meteorological conditions, either directly by the wind speed or indirectly through the influence of precipitation on soil

moisture, surface composition and land use (Yahi et al., 2013). Moreover, dust particles have been identified to change the radiation balance both at the regional and local scales especially because large dust-lifting events occur frequently in this region (Slingo et al., 2006, 2008; Solomon et al., 2008).

Dust aerosols may influence regional climate through a direct effect by scattering and absorbing solar radiation which leads to warming (cooling) of the atmospheric layers in the case of absorption (reflection) respectively (Quijano et al., 2000; Miller et al., 2004; Fast et al., 2006; Péré et al., 2011; Ma et al., 2012; Heald et al., 2014; Nabat et al., 2015; Graaf et al., 2019). Absorbing particles through a semi-direct effect may limit cloud formation by reducing the adiabatic cooling of the atmosphere as absorbing particles heat the cloud layer and cause cloud

* Corresponding author.

E-mail address: xma@nuist.edu.cn (X. Ma).

<https://doi.org/10.1016/j.jastp.2020.105213>

Received 4 May 2019; Received in revised form 2 January 2020; Accepted 23 January 2020

Available online 27 January 2020

1364-6826/© 2020 The Authors.

Published by Elsevier Ltd.

This is an open access article under the CC BY-NC-ND license

(<http://creativecommons.org/licenses/by-nc-nd/4.0/>).

evaporation (Koch and Del Genio, 2010; Nabat et al., 2015; Amiri-Farahani et al., 2017; Allen et al., 2019; Amiri-Farahani et al., 2019). Furthermore, aerosol particles may have a significant impact on precipitation and radiation budget by modifying the albedo and the lifetime of the cloud (Twomey, 1977; Haywood and Boucher, 2000; Sekiguchi et al., 2003; Lohmann and Feichter, 2005; Gu et al., 2012).

Many studies have been conducted on aerosol climatology using direct ground-based atmospheric observations and climate models over the past decades to improve our understanding of the spatiotemporal variability, heterogeneity and spectral varying behavior of aerosols (Slingo et al., 2006; Otto et al., 2007; Ma et al., 2012; Kokkalis et al., 2018). Ground-based atmospheric observations focus on field campaigns mainly in regions considered as major dust sources (Kim et al., 2009; Marticorena et al., 2010, 2017). Over the years, many scientific efforts have been dedicated to increasing and improving field campaigns by installing networks of aerosol observations in selected sites around the World. These selected sites usually over semi-arid and desert areas have been used in global and regional studies (García et al., 2012; Kokkalis et al., 2018). However, ground-based atmospheric observations possess some inherent limitations when used at global and regional scales (Holben et al., 1998). This is largely due to the low stations (or measurements) density, limited spatial coverage and lack/poor of maintenance, particularly in developing countries.

Climate models are developed to resolve this limitation and have been applied in many modeling studies to estimate the dust balance (Haustein et al., 2015; Flaounas et al., 2017; Eltahan et al., 2018; LeGrand et al., 2019). However, climate models produce uncertainties that are difficult to quantify (Nicholson, 2000) and some of these uncertainties may be attributed to the variety of dust emission schemes and model configurations such as initial and lateral boundary conditions for meteorological fields and surface properties. In most cases, these uncertainties degrade the quality of output in these climate models for quality monitoring and evaluation purposes particularly in regions with poor or inconsistent monitoring and measuring of direct ground-based observations. Important progress has been made in satellite technology and numerical dust models in assessing the temporal and spatial variability of dust from North Africa, but uncertainties still exist for practically all stages of the dust cycle (Hoff and Christopher, 2009; Knippertz and Todd, 2010; Adams et al., 2012; Fiedler et al., 2013, 2014; Evan et al., 2015, 2016; Graaf et al., 2019; Voss and Evan, 2019).

The present study evaluates the dust emission schemes within WRF-Chem in simulating dust content and extinction coefficient with CALIPSO satellite-based and AERONET ground-based observations in northern Africa during the summer of 2006. The remaining article is structured as follows: Section 2, the study methodology gives a description of the models and experimental setup used in the study. Section 3 provides results and discussion from the evaluation of the model-based estimates compared against observation data. The conclusions are presented in Section 4.

2. Methodology

2.1. Model description and experiment setup

The Weather Research and Forecasting model coupled with chemistry (WRF-Chem) is a fully coupled meteorology-chemistry-aerosol model with the ability to simulate simultaneously the emission, transport, deposition, mixing and chemical transformation of trace gases, aerosol interactions, photolysis and radiation with meteorology (Grell et al., 2005). Cloud chemistry, aerosol-cloud interactions, and their feedback processes were incorporated into the WRF-Chem (Fast et al., 2006; Chapman et al., 2009). In this study, version 4.0.2 of the WRF-Chem implements three different dust emission schemes, which include emission, advection, and deposition. The three dust schemes include the Goddard Global Ozone Chemistry Aerosol Radiation and Transport (GOCART) originally described by Ginoux et al. (2001, 2004),

the Air Force Weather Agency (AFWA) (Jones et al., 2012), and the University of Cologne (UoC) described by Shao, 2001, 2004; Shao et al. (2011).

All the three-dust emission schemes were run in their default configuration in the WRF-Chem model version 4.0.2. All three schemes compute also dust emission as a function of wind energy, soil moisture, and particle size, and use the same erodible soil particles, called dust source function to represent the availability of loose erodible soil material (LeGrand et al., 2019). The main physical mechanisms of dust lifting which are the threshold friction velocity of wind erosion, the saltation bombardment and the disintegration of the aggregates are considered in the three-dust emission schemes. The threshold friction velocity of wind erosion is the velocity at which dust particles can be lifted from the surface directly by wind shear forces. Saltation bombardment occurs when sand particles or aggregates strike the surface, causing localized impacts that are often strong enough to overcome the binding forces acting on the dust particles, resulting in significant dust emission (Gillette, 1981; Kok et al., 2012; Scanza et al., 2015). During severe wind erosion, dust layers attached to sand grains in sandy soils or as aggregates in soils with high clay content initially difficult to release by low wind erosion can disintegrate causing increased emission of dust, this process is called the disintegration of aggregates.

Dust emission flux in each scheme, are then distributed into five different *size bins* with an effective particle radius of 0.5, 1.4, 2.4, 4.5 and 8.0 μm . The emission within each bin is injected to the lowest atmospheric model level, and the chemical module computes the dispersion. Separate schemes are used to estimate dust mass concentrations for transport and removal from the atmosphere (LeGrand et al., 2019). The Mie theory is used to calculate optical properties, by assuming dust particles to be spherical and internally mixed in each size bins as described by Barnard et al. (2010). We recognized that spherical assumption of dust particles may lead to significant uncertainty due to the non-spherical nature of these particles which may result in model bias (Kalashnikova and Sokolik, 2002; Schladitz et al., 2009; Kok et al., 2017).

The optical properties are calculated as a function of wavelength at each model grid point for wavelengths of 300 nm, 400 nm, 600 nm and 999 nm following Barnard et al. (2010), i.e. the aerosol optical thickness (AOD), the single scattering albedo (SSA), the asymmetry parameter (g). A constant value of dust refractive index for SW radiation is used for real and imaginary refractive indices of 1.55 and 0.006 for the four short-wave spectral bands of 300 nm, 400 nm, 600 nm, and 999 nm. However, the refractive indices of dust for longwave radiation are considered to be wavelength dependent and vary for 16 longwave bands. The refractive indices are calculated by volume averaging for each aerosol size bin. The optical properties of dust aerosols are determined by interpolation at the wavelength of the centers of the band located between the four wavelengths. The Angstrom relationship is used to determine aerosol extinction and linear interpolation for single scattering albedo and the asymmetry parameter. The modeled AOD at 550 nm wavelength and the exponent of Angstrom α is calculated according to the formula:

$$AOD(550) = AOD(400) * \left(\frac{550}{400}\right)^\alpha \quad (1)$$

$$\text{with } \alpha = \frac{\ln\left(\frac{AOD(400)}{AOD(600)}\right)}{\ln\left(\frac{600}{400}\right)}$$

Table 1 lists the main physical and chemical options used in this study. The cloud microphysical scheme (Lin et al., 1983) that includes ice, snow and graupel processes, suitable for high-resolution simulations with real data was used. The Rapid Radiative Transfer Model (RRTMG) scheme (Iacono et al., 2008) that includes the Monte Carlo independent column approximation (MCICA) method of random cloud overlap was used for both Longwave (LW) and Shortwave (SW) radiations. The

Table 1

Physical and chemical modeling options used in this study.

Option	Number	Model
Microphysics	2	Lin et al. (1983) scheme
Longwave Radiation	4	RRTMG
Shortwave Radiation		
Surface Layer	1	MM5 Similarity Scheme
Land Surface	2	Unified Noah Land Surface Model
Planetary Boundary layer	1	Yonsei University Scheme (YSU)
Cumulus Parameterization	5	Grell 3D Ensemble Scheme
Chemistry	300	GOCART simple aerosol scheme
Dust emission	1	Includes GOCART
	3	Includes AFWA
	4	Includes UoC following Shao (2004)

planetary boundary layer was chosen by the non-local K scheme of Yonsei University with an explicit training layer and a parabolic K profile in an unstable mixing layer (Hong et al., 2006). This scheme includes topographic correction for surface winds to represent additional drag due to sub-grid topography and increased flow at the top of a hill and an option for descending mixture driven by radiative cooling. The cumulus parameter setting option (Grell, 1993; Grell and Dévényi, 2002) chosen is Grell 3D, an improved version of the GD scheme. Noah's land surface model with four-layer temperature and soil moisture, split snow cover, and frozen soil physics was selected (Mukul Tewari et al., 2004). Finally, the Monin-Obukhov-based MM5 similarity scheme with the Carlson-Boland viscous underlayer and the standard similarity functions from the look-up tables was used (Paulson, 1970; Dyer and Hicks, 1970; Webb, 1970; Zhang and Anthes, 1982; Beljaars, 1995).

In this study, three simulations are conducted from May 22 to August 31, 2006, with the first 10 days as the model spin-up time, and an adaptive time step was used for numerical stability. This period was chosen because Saharan aerosols predominate during summer months when dust events are associated with strong convective events (Prospero, 1996; Jones et al., 2003; Engelstaedter et al., 2006). Our aim is to examine the ability of each dust emission scheme in simulating dust content and the extinction coefficient during the summer of 2006 over

the north of Africa. The model is configured to cover north of Africa as illustrated in Fig. 1, indicating the location of countries and the main Saharan mountains with 202×140 grid points at 30 km horizontal resolution and 51 vertical levels following a stretched sigma-coordinate system for high vertical resolution near the surface, covering the whole troposphere (up to 5000 Pa). The used of vertical resolution greater than the commonly used (30–40 levels) may reduce bias in model simulations and better depicts the small scale extinction coefficient patterns often associated to regions of high concentration gradients of aerosols and where local and small scale processes are dominant such as North Africa (Teixeira et al., 2016). The model is initialized with zero dust concentration transported into the domain across the lateral boundaries during the simulations. The main limitation of this approach is to allow the model to generate, build up, and transport its own dust and as known dust plumes lifetime can go beyond a few days or even weeks. This cannot impact the results but it can affect the model output for short-range dust predictions, up to 48 h (Alpert et al., 2002).

Initial and lateral boundary conditions for meteorological fields are provided by the National Environmental Prediction Center (NCEP) 1-degree resolution re-analysis data. The sea surface temperature was updated in the three simulations using data downloaded from NOAA/National Weather Service National Centers for Environmental Prediction Environmental Modeling Center server (<ftp://polar.ncep.noaa.gov/pub/history/sst/>). All three simulations used also the same physics options. Convective transport of aerosols by cumulus clouds is based on the Grell convection scheme (Grell and Dévényi, 2002) and the representation of vertical turbulent mixing by a first-order K-theory scheme based on non-local boundary layer vertical diffusion of Yonsei University (Hong et al., 2006). Dry deposition includes gravitational settling and surface deposition (Wesely, 1989). Wet deposition is not considered in the simulations, and this can increase the concentration of the dust particles in the model. The SW and photolysis schemes are considered to include the effects of unresolved clouds as well as the direct and semi-direct effects of dust. All simulations are unaffected by dust indirect effects and biomass burning emissions. The main chemical modeling options used are listed in Table 1.

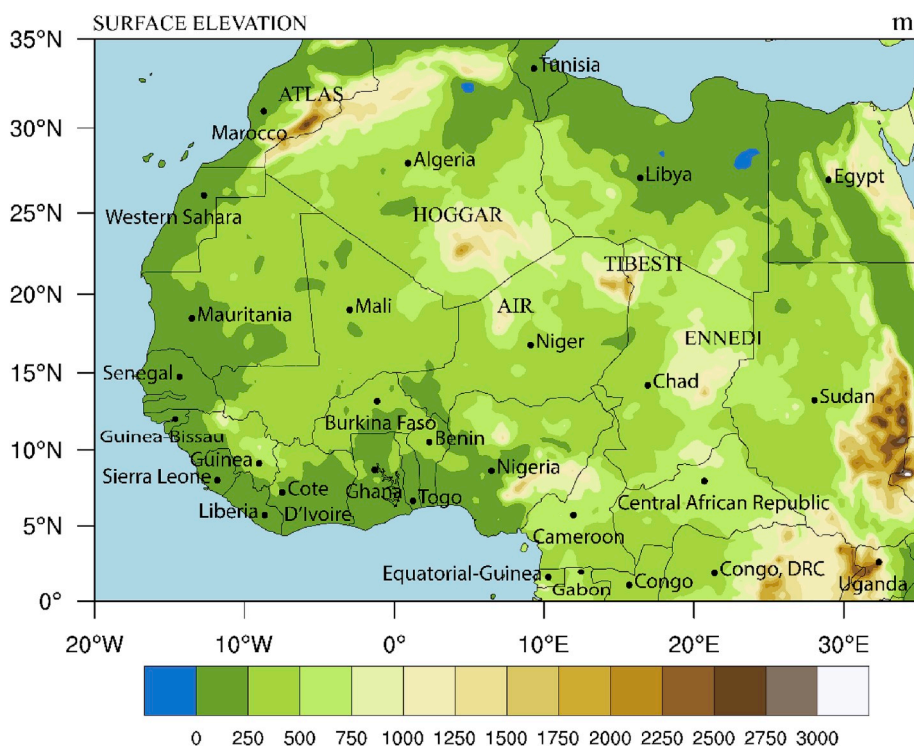


Fig. 1. Model domain with the location of countries included in the study area superimposed on the surface elevation topography (m).

2.2. Dust emission schemes

Within the WRF-Chem model, complex dust emission processes are represented by an empirical source function S established by [Ginoux et al. \(2001\)](#) based on physical characteristics of the land surface:

$$S = \left(\frac{Z_{max} - Z_i}{Z_{max} - Z_{min}} \right)^5 \quad (2)$$

where S is the probability value to have accumulated sediments in the i th grid cell of altitude Z_i , and Z_{max} and Z_{min} are the maximum and minimum elevations in the surrounding $10^\circ \times 10^\circ$ topography, respectively. The S values are set to zero anywhere bare soil is not indicated by data derived from the Advanced Very High-Resolution Radiometer (AVHRR) product and interpolated to the model grid ([Defries and Townshend, 1999](#)).

The first scheme used in this study is GOCART. In this scheme, the dust emission flux (F_p) values for each size bin were obtained using the similar empirical formula developed by [Gillette and Passi \(1988\)](#), given below by:

$$F_p = \begin{cases} CSs_p u_{10m}^2 (u_{10m} - u_t) & \text{if } u_{10m} > u_t \\ 0 & \text{otherwise} \end{cases} \quad (3)$$

where C is a dimensional factor equal to $1 \mu\text{gs}^2 \text{m}^{-5}$, S is the source function described by [Ginoux et al. \(2001\)](#) (the same in equation (2)) representing the fraction of alluvium available for wind erosion. u_{10m} is the horizontal wind speed at 10 m, u_t is the threshold 10 m wind velocity for initiating erosion, and s_p is the mass fraction of each size class of dust emission. u_t is original from ([Bagnold, 1941](#)) and now from [Marticorena and Bergametti \(1995\)](#) in the WRF-Chem model.

The threshold velocity for dust production is the most important parameter of the formula due to its dependence on the effects of vegetation residue, soil roughness, soil texture and the effect of atmospheric precipitation ([Gillette and Passi, 1988](#)).

The second dust emission scheme is the Air Force Weather Agency (AFWA). AFWA is based on [Marticorena and Bergametti \(1995\)](#) and is composed of three main components including the threshold friction velocity, saltation flux, and bulk vertical dust flux.

Threshold Friction Velocity is given following [Iversen and White \(1982\)](#) and is written as follows:

$$u_t(D_p) = 0.129 \frac{\left[\frac{\rho_p g D_p}{\rho_a} \right]^{0.5} \left[1 + \frac{0.006}{\rho_p g D_p^2} \right]}{\left[1.928 (aD_p^x + b) - 1 \right]^{0.5}} \quad u_t = u_t(D_p) \frac{f(\text{moisture})}{f(\text{roughness})} \quad (4)$$

where g is gravitational acceleration; D_p is particle diameter; ρ_a is air density; $aD_p^x + b$ is the friction Reynolds number with $a = 1331$, $b = 0.38$, and $x = 1.56$.

Saltation Flux over Bare Soil ([Kawamura, 1951](#)): the dust flux is quantified through saltation flux as,

$$H(D_p) = C \frac{\rho_a}{g} u^3 \left(1 + \frac{u_t}{u} \right) \left(1 - \frac{u_t^2}{u^2} \right) \quad (5)$$

where C is an empirical constant, ρ_a is the density of air parcel, g is the acceleration due to gravity, u and u_t are, respectively, friction velocity and threshold friction velocity. The friction velocity is considered instead of horizontal wind speed at 10 m as in the GOCART scheme.

Bulk Vertical Dust Flux ([Gillett, 1979](#)): the concentration of elevated dust triggered by saltation is explained by the following expression

$$F_{bulk} = H\alpha \times S \quad \alpha = 10^{0.134(\% \text{clay}) - 6} \quad (6)$$

where α is the sandblasting efficiency factor and S is the dust erodible

surface fraction described by [Ginoux et al. \(2001\)](#) (the same in equation (2)). %clay is the soil clay content mass fraction determined from the FAO-SMW data.

The difference between the GOCART and AFWA emission schemes is in how the dust emission flux is calculated in each scheme ([LeGrand et al., 2019](#)). In AFWA, a bulk vertical dust flux is calculated and then distributed into the suspended dust size bins following the theory of [Kok \(2011\)](#), whereas in GOCART, the dust emission flux is calculated separately for each of the five dust bins.

The third scheme used is the University of Cologne (UoC). The UoC provides three versions of dust emission schemes based on [Shao, 2001, 2004; Shao et al. \(2011\)](#). The UoC scheme following [Shao \(2004\)](#) is used in this study, which is a moderate simplification of the dust emission scheme proposed by [Shao \(2001\)](#), which is somewhat complicated to use in practice. It also incorporates physically-based aggregate disintegration algorithms not included in the [Shao et al. \(2011\)](#) setting and has less dependency on soil attributes than ([Shao, 2001](#)). In the UoC scheme following [Shao \(2004\)](#), the dust emission is generated by the saltation bombardment and aggregates disintegration and therefore the rate of dust emission is proportional to the flow of saltation flux.

$$F(d_i, d_s) = C_\gamma \eta_{fi} [(1 - \gamma) + \gamma \sigma_p] (1 + \sigma_m) \frac{gQ}{u_*^2} \quad (7)$$

where $F(d_i, d_s)$ is dust emission rate for the i th particle group of size d_i generated by the saltation of particles of size d_s ; c_γ is a dimensionless coefficient and γ is a function that describes how easily aggregated dust can be released specified as

$$\gamma = \exp[-(u_* - u_{*t})^3] \quad (8)$$

Q is the streamwise saltation flux of d_s ; g is acceleration due to gravity and u_* is friction velocity; u_{*t} is the threshold friction velocity; σ_m is the ratio between m (mass of impacting particle) and m_Ω (mass ejected by bombardment), i.e.,

$$\sigma_m = \frac{m_\Omega}{m} \quad (9)$$

which can be interpreted as bombardment efficiency; σ_p is free dust to aggregated dust ratio, i.e.,

$$\sigma_p = \frac{\eta_{mi}}{\eta_{fi}} = \frac{P_m(d_i)}{P_f(d_i)} \quad (10)$$

The threshold friction velocity in the UoC is calculated by the similar function used in the AFWA scheme with additional corrections for surface drag effects based on the fraction of vegetation within the model grid cell.

The three schemes use the same dust source function by default as defined by [Ginoux et al. \(2001\)](#) over North Africa within the model used in this study (see [Fig. 2a](#)). The GOCART and AFWA schemes use the dust source function as a scale factor to reduce dust emissions (dust emissions parametrized as a function of atmospheric and soil physical properties are scaled in each grid point with values between 0 and 1), while the UoC scheme uses the dust source function to define areas of potential dust emission (dust emissions are calculated only at grid points where erodibility is non-zero).

2.3. Observational data

The first data used in this study is Cloud-Aerosol Lidar and Infrared Pathfinder Satellite Observations (CALIPSO) Level 3 aerosol product ([Winker et al., 2013](#)), monthly gridded datasets at $2^\circ \times 5^\circ$ resolution derived from the CALIPSO Lidar Level 2 aerosol profile cloud-free standard. The nighttime dust optical depth (AOD) and dust extinction coefficient at 532 nm data are used since the return signals are significantly better quality than during daytime when the signal-to-noise ratio is affected by the sunlight ([Powell et al., 2009; Adams et al., 2012; Ma](#)

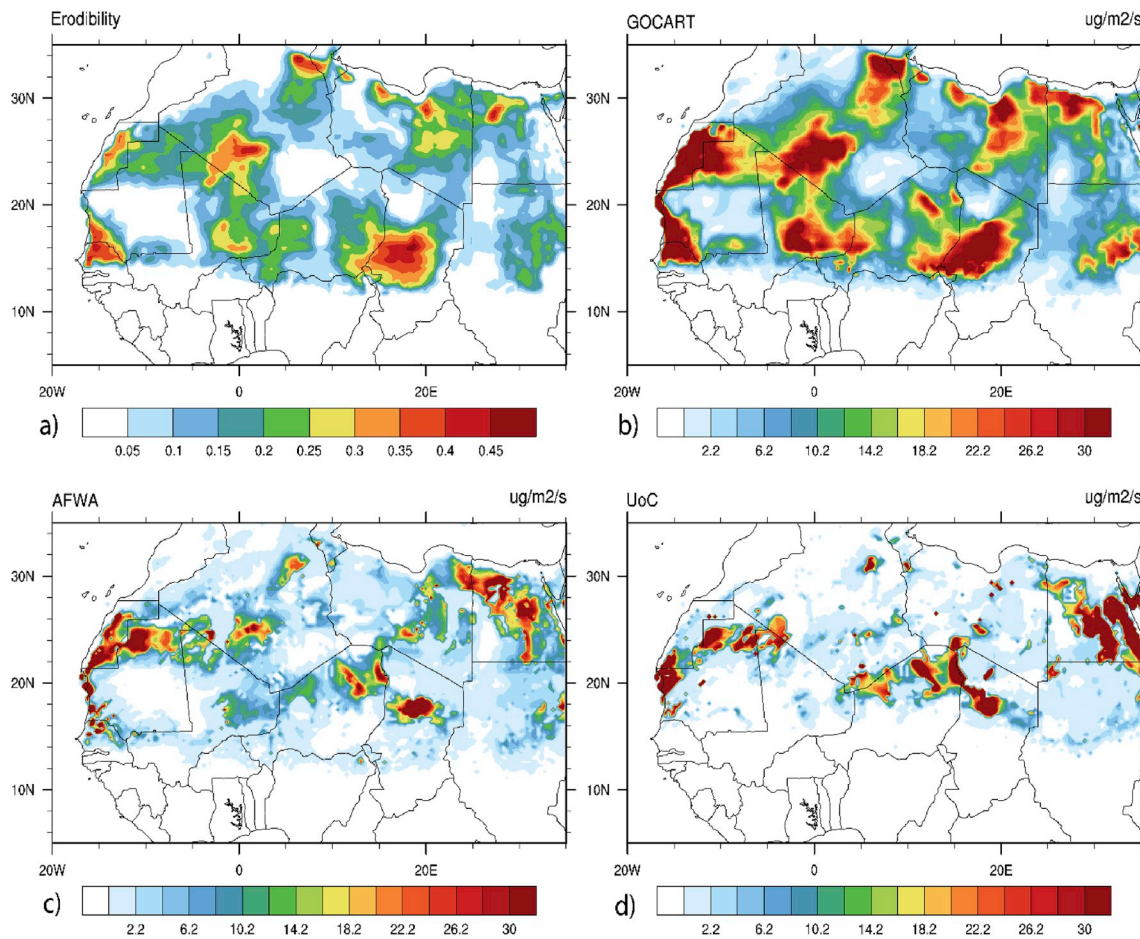


Fig. 2. a) Dust erodibility from the Weather Research and Forecasting model coupled with chemistry (WRF-Chem). Total dust emission ($\mu\text{g}/\text{m}^2/\text{s}$) averaged over June July August 2006 simulated by the Weather Research and Forecasting model coupled with chemistry (WRF-Chem), from b) the Goddard Global Ozone Chemistry Aerosol Radiation and Transport (GOCART) scheme, c) the Air Force Weather Agency (AFWA) scheme, and d) the University of Cologne (UoC) scheme.

et al., 2013). CALIPSO is a satellite developed within the framework of a collaboration between NASA and the French Space Agency CNES (Center National d'Etudes Spatiales) launched in 2006 (Winker et al., 2007). The CALIPSO's main instrument is Cloud-Aerosol Lidar with Orthogonal Polarization (CALIOP) that provides vertical profiles of aerosol and cloud backscatter, and depolarization with two spectral channels (532 nm and 1064 nm) and equipped with a 1-m diameter telescope (Winker et al., 2004). The other two instruments are a Wide-Field Camera (WFC), which acquires science data only under daylight conditions and a 3-channel Infrared Imaging Radiometer (IIR) for the retrievals of cirrus particle size.

The second data used are the measurements from three Aerosol Robotic Network (AERONET) stations (Holben et al., 1998). The locations of these stations are summarized in Table 2 (see also Fig. 4), the high-quality Level 2.0 data from version 3 were acquired from the AERONET website (<http://aeronet.gsfc.nasa.gov>). To compare with model outputs, AOD was calculated at 550 nm using Angström exponent relationship for all stations.

Table 2
Locations of AERONET stations used in this study.

Station	Location	Lat	Lon	Alt (m)	Geo location
Banizoumbou	Niger	13.5 N	2.6 E	274	Semi-Arid
Cinzana	Mali	13.2 N	5.9 W	285	Semi-Arid
MBour	Senegal	14.3 N	16.9 W	21	Coastal

3. Results and discussion

3.1. Dust emissions

Fig. 2a shows the fraction of alluvium available for soil wind erosion in the WRF-Chem model and is defined as the dust source function by Ginoux et al. (2001) as based on the physical characteristics of the land surface. Fig. 2b, c, and d show the spatial distribution of total dust emission flux from simulations with GOCART, AFWA and UoC schemes, respectively averaged over the simulation period in North Africa. All three schemes generally simulate a coherent distribution of total dust emissions that occur mainly in the desert regions of the Sahara ($15^\circ\text{N} - 35^\circ\text{N}$) in North Africa during the simulation period. GOCART simulates the major dust emission source regions similar to the source function, which are extended from Western Sahara to Libya, including the north and south-west of Mauritania, north Mali, and west and east Algeria. The Bodélé depression source in the Saharan Sahel region is located between the Air massifs (maximum altitude 2022 m) and Tibesti (3415 m) and covers regions of Niger and Chad.

In contrast, AFWA and UoC schemes simulate almost similar spatial distribution, which is different from GOCART in terms of extent, magnitude and pattern. This is due to the calculation of the threshold friction velocity in which the soil moisture correction factor is calculated differently than in GOCART, using a modified version of the correction function (LeGrand et al., 2019). The temporal daily mean distribution of the total dust emissions on the three schemes over the simulation period in North Africa is shown in Fig. 3. The GOCART scheme emits more dust flux over the simulation period but shows good consistency with the

AFWA and UoC schemes given a correlation of 0.5 for both AFWA and UoC. Though, the AFWA and UoC schemes are well correlated with a correlation coefficient of 0.8. This indicates the dominant influence of the simulated 10 m wind speed and the friction velocity on the temporal distribution of dust emissions between GOCART and the other two schemes (AFWA and UoC).

3.2. Distribution of AOD on the regional scale

Fig. 4 presents the spatial distribution of dust AOD at 532 nm obtained from the CALIPSO (Fig. 4a) and simulations by the three dust emission schemes in WRF-Chem - GOCART (Fig. 4b), AFWA (Fig. 4c) and UoC (Fig. 4d) averaged over the study area during summer 2006. For comparison purposes, the modeled AOD from the three dust emission schemes is sampled at the same overpass time as CALIPSO nighttime dust AOD. The results generally show a uniformity of AOD between CALIOP and the three dust emission schemes in the model. Higher values of AOD extracted from CALIOP are observed over West Africa between 15 °N and 25 °N with the maximum located over Mauritania, Mali and southern Algeria. All three dust emission schemes failed to reproduce correctly the maximum zones of observed AOD by CALIOP. The GOCART and AFWA scheme present similar patterns and extent over West Africa while the UoC scheme shows localized AOD over the Sahel region from the Atlantic Ocean to the north of Sudan. In the Sahel region, the Bodélé depression on the border Chad-Niger south of the Tibesti massif experienced a higher peak for the three schemes than that observed in CALIOP.

3.3. Distribution of AOD at the local scale

The daily evolution of modeled AOD from the three dust emission schemes is compared against the AERONET observations at the sites of Banizoumbou in Niger, Cinzana in Mali and M'Bour in Senegal during the summer of 2006 (see Fig. 5). The AERONET AOD were interpolated to 550 nm using Angström exponent relationship between 440 nm and 675 nm for all three stations during the summer of 2006. The choice of these AERONET sites (Banizoumbou, Cinzana, M'Bour) is due to their location close to the sources and or on the transport axis of the Saharan aerosols. The model's ability to reproduce AERONET observations are estimated by metrics summarized in Table 3 and are defined as.

– correlation,

$$\frac{\sum_{i=1}^n (X_{obs,i} - \bar{X}_{obs}) \cdot (X_{model,i} - \bar{X}_{model})}{\sqrt{\sum_{i=1}^n (X_{obs,i} - \bar{X}_{obs})^2 \cdot \sum_{i=1}^n (X_{model,i} - \bar{X}_{model})^2}} \quad (11)$$

– bias,

$$\frac{1}{n} \sum_{i=1}^n (X_{obs,i} - X_{model,i}) \quad (12)$$

– normalized bias,

$$\frac{\frac{1}{n} \sum_{i=1}^n (X_{obs,i} - X_{model,i})}{\bar{X}_{obs}} * 100 \quad (13)$$

– root mean square error,

$$\sqrt{\frac{\sum_{i=1}^n (X_{obs,i} - X_{model,i})^2}{n}} \quad (14)$$

– normalized root mean square error.

$$\sqrt{\frac{\sum_{i=1}^n (X_{obs,i} - X_{model,i})^2}{n}} \cdot \frac{100}{\bar{X}_{obs}} \quad (15)$$

where $X_{obs,i}$ is an observed variable, $X_{model,i}$ is a modeled variable, the upper bar represents the average of overall data, and "n" is the total number of locations that the predicted data is compared to against the observations.

Fig. 6 shows the Taylor diagram in addition to the statistics used for time series in Fig. 5. All the three schemes show a similar daily temporal pattern with observations made by AERONET stations but are not well agreed in reproducing different peaks of AOD over the study period. Some peaks are simulated only slightly in advance or delay to

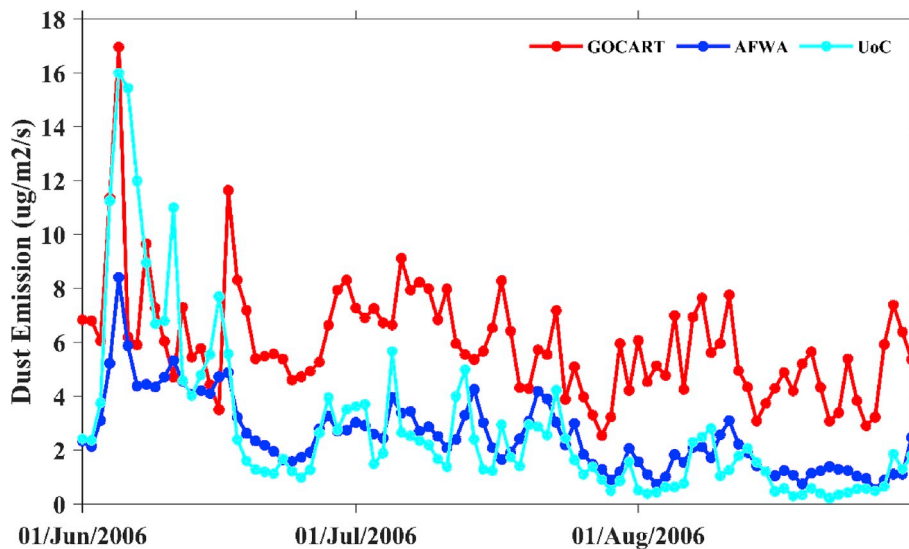


Fig. 3. Daily mean total dust emission ($\mu\text{g}/\text{m}^2/\text{s}$) over June July August 2006 simulated by the Weather Research and Forecasting model coupled with chemistry (WRF-Chem), from the Goddard Global Ozone Chemistry Aerosol Radiation and Transport (GOCART) scheme, the Air Force Weather Agency (AFWA) scheme and the University of Cologne (UoC) scheme.

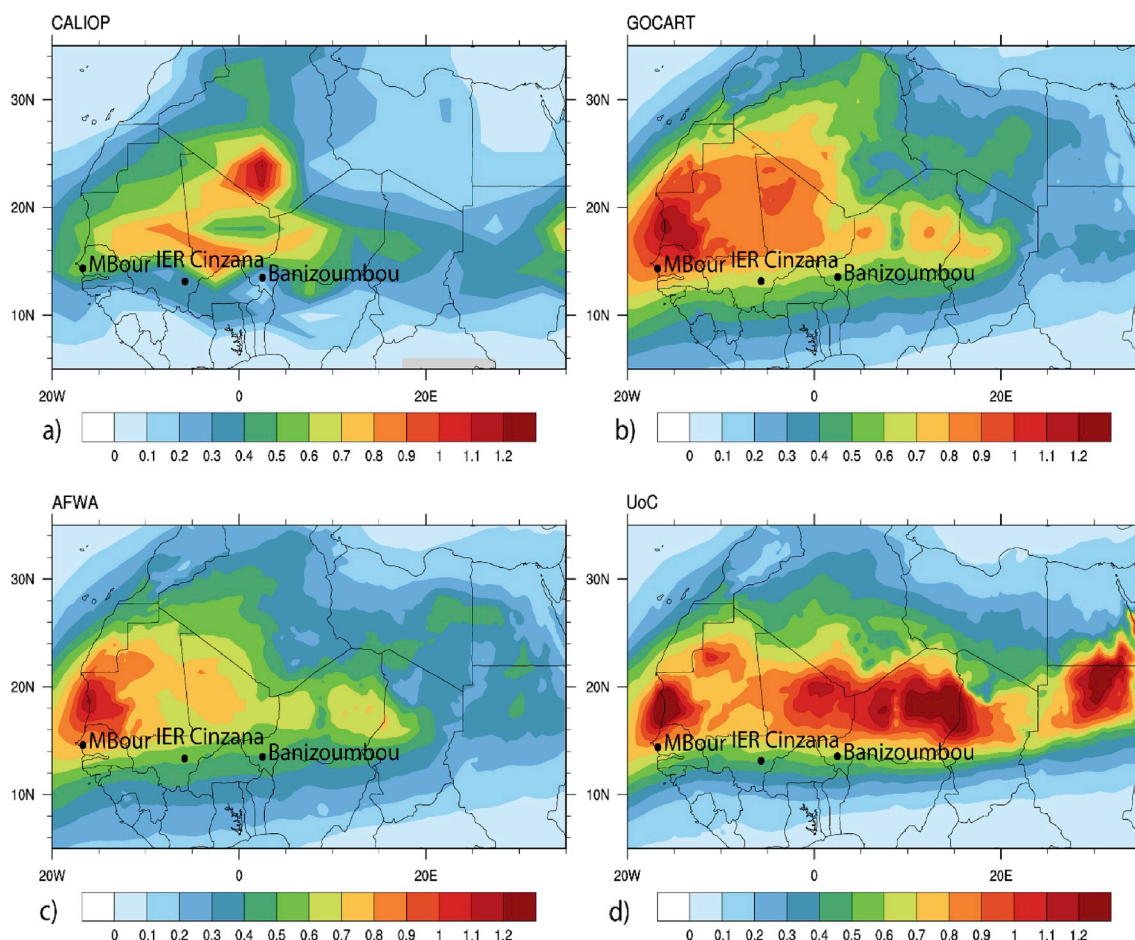


Fig. 4. Dust optical depth averaged over June-July-August 2006, from a) the CALIOP at 532 nm, and the simulated at 550 nm, by the Weather Research and Forecasting model coupled with chemistry (WRF-Chem), from b) the Goddard Global Ozone Chemistry Aerosol Radiation and Transport (GOCART) scheme, c) the Air Force Weather Agency (AFWA) scheme, and d) the University of Cologne (UoC) scheme. The locations of the three AERONET sites (Banizoumbou, Cinzana and M'Bour) are indicated.

observations. As can be seen, high daily observed AOD values are recorded in Banizoumbou (Fig. 5a) and Cinzana (Fig. 5b) than in M'Bour station (Fig. 5c). The maximum daily AOD is lower in M'Bour (up to 1.2) than in Banizoumbou (up to 2.1) and slightly higher in Cinzana (up to 2.4). In their work, Menut et al. (2013) were found similar results by investigating the impact of surface roughness and soil texture on mineral dust emission fluxes modeling. They measured also high values of AOD in Banizoumbou and Cinzana stations, with observed peaks reaching values up to 2 and can be explained by the proximity of these stations to mineral dust sources. Schmechtig et al. (2011) simulated mineral dust content over Western Africa from the event to the annual scale with the CHIMERE-DUST model. They recorded high peaks of AOD observed during the summer of 2006 in Banizoumbou and Cinzana than in M'Bour station which recorded only a few of these events. Simulating correctly the daily variation of AOD is very challenging because dust events are influenced by local convective events at the beginning of the rainy season (Marticorena et al., 2010). In the three stations, dust events occur by several peaks over the study period. This happens when dust sources are activated, such as northern Senegal, in Mauritania and in Western Sahara for the M'Bour station, in the north-central Sahara, the northern Niger and Bodele depression regions for the other two stations (Banizoumbou and Cinzana) (Fig. 4).

All the three schemes reproduce the increase of AOD in the middle of June during the beginning of the West African monsoon for the three AERONET stations (Fig. 5). Although, the GOCART and AFWA schemes underestimate the peaks in the middle of June in Banizoumbou and Cinzana stations, while the UoC scheme overestimates it (Fig. 5a). All

the three schemes overestimate the increase of AOD in the middle of June in M'Bour station (Fig. 5c). The UoC scheme presents lower values of daily AOD from the end of July to the end of August than the other two schemes (GOCART and AFWA) for all the three AERONET stations. The simulation with GOCART shows a lower correlation coefficient of 0.32 than AFWA and UoC, which show a correlation coefficient of 0.63 and 0.8 in Banizoumbou station, respectively. The UoC and AFWA schemes are better correlated than the GOCART scheme in Banizoumbou station. GOCART simulation has the lowest normalized bias of 2% than the other two Scheme 13% and -5% for both UoC and AFWA simulation, respectively. Normalized root mean square error of 47% is obtained for the AFWA scheme simulation, 55% for the UoC scheme and 88% for the GOCART scheme simulation. The AFWA and UoC schemes perform better in terms of high correlation values compared to the GOCART scheme. The AFWA scheme is also much closer to the observation in terms of intensity indicated by the standard deviation shown in the Taylor Diagram for the Banizoumbou station (Fig. 6a).

The three schemes simulations show poor correlation with the observation in Cinzana station (Fig. 5b). The UoC scheme is better correlated than the two other schemes (GOCART and AFWA) with a correlation coefficient of 0.55. Simulations with GOCART and AFWA schemes show a correlation coefficient of 0.24 and 0.38, respectively. The GOCART simulation has a normalized bias of -13%, AFWA and UoC scheme simulations indicate a normalized bias of 5% and 4%, respectively. Normalized root mean square error of 75% is estimated for the GOCART simulation, 58% and 93% for the AFWA and UoC simulation, respectively. The UoC scheme performs better in terms of correlation

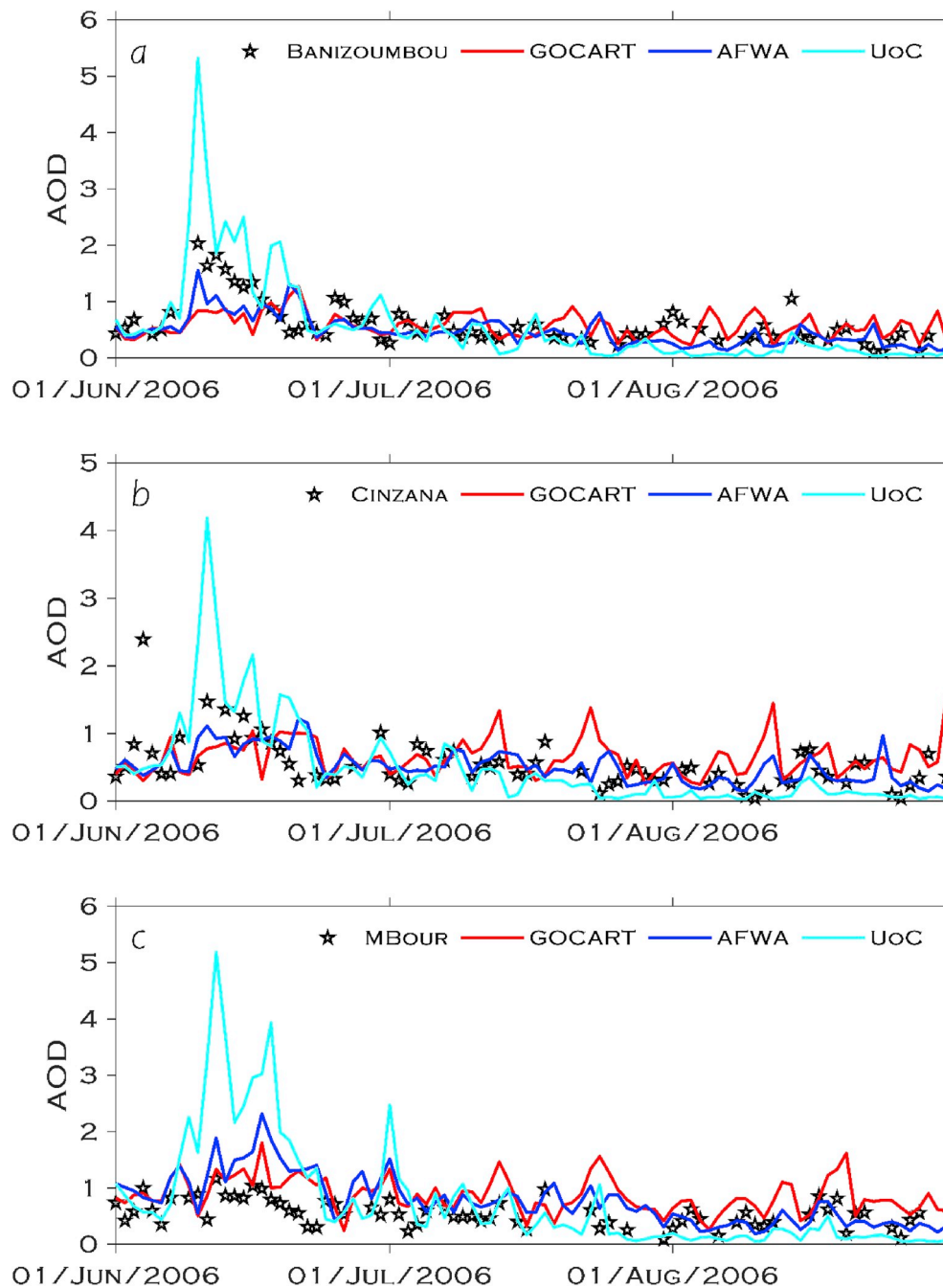


Fig. 5. Time series of daily AOD values over June–July–August 2006, from AERONET observations (Banizoumbou, Cinzana, M’Bour) at 550 nm, and simulated by the Weather Research and Forecasting model coupled with chemistry (WRF-Chem), from the Goddard Global Ozone Chemistry Aerosol Radiation and Transport (GOCART) scheme, the Air Force Weather Agency (AFWA) scheme and the University of Cologne (UoC) scheme.

and normalized bias but has a large percentage of normalized root mean square error compared to the other two schemes (GOCART and AFWA). AFWA is also much closer to the observation in terms of the intensity observed from the Taylor diagram by standard deviation shown in Fig. 6b. Briant et al. (2017) using online coupling between the WRF meteorological model and the Chapman et al., 2009 chemistry-transport model, calculated low correlation in Cinzana (0.23–0.29), Banizoumbou (0.37–0.44). They showed that the two stations (i.e. Banizoumbou, Cinzana) present lower performances due to the difficulty in reproducing dust events within the model, as dust is the main AOD contributor at these stations.

The M’Bour station (Fig. 5c) presents small values of AOD than the other two previous mentioned stations (Banizoumbou and Cinzana). All

the AOD values are below 1.2 over the study period at the M’Bour station (Fig. 5c). A correlation of 0.59 is obtained for the AFWA and 0.58 for the UoC scheme simulations while the GOCART simulation shows a correlation of 0.38 compared to observations made at the M’Bour station (Fig. 5c). The AFWA simulation has the smallest normalized bias of –36% while GOCART and AFWA simulations show a normalized bias of –45% and –48%, respectively. Normalized root mean square error of 72% is estimated for the GOCART simulation, 71%, and 159% for the other two schemes (AFWA and UoC) simulations, respectively. The AFWA and UoC schemes are well correlated with the observation at the M’Bour station than the GOCART scheme. In terms of the intensity indicating by the standard deviation in the Taylor diagram (Fig. 6c), the GOCART scheme is closer to the observation. The differences between

Table 3

Estimation of model's ability to reproduce AERONET observations using the correlation coefficient, the normalized bias and the normalized root mean square error.

	Correlation (R)	Normalized bias (%)	Normalized Root Mean Square Error (%)
Banizoumbou			
GOCART	0.32	2	55
AFWA	0.63	13	47
UoC	0.8	-5	88
Cinzana			
GOCART	0.24	-13	75
AFWA	0.38	5	58
UoC	0.55	4	93
M'bour			
GOCART	0.38	-45	72
AFWA	0.59	-36	71
UoC	0.58	-48	159

the M'bour and the other two stations are due to their geographical location and precipitation conditions (Marticorena et al., 2010). The M'bour station has the lowest annual precipitation but the vegetation cover is much higher due to its proximity to the coastal area than in the two other stations (Banizoumbou and Cinzana). The Banizoumbou station is closer to active dust sources such as the Bodele depression and is situated in a more arid area than the Cinzana station.

3.4. Vertical profile of dust extinction coefficient

The simulated dust extinction coefficient profiles at 550 nm from the three emission schemes are compared against the CALIOP observation in Fig. 7 (averaged over 20 °W and 35 °E). The higher values of dust extinction coefficient are observed in the lower layers and can be lifted up to 5 km with maximums below 1 km between 10 °N and 30 °N by CALIOP vertical profile (Fig. 7a). The three dust emission schemes simulations (Fig. 7b, c, and 7d) reproduce broadly the pattern and intensity of dust extinction coefficient profile of CALIOP. All simulations overestimate also the vertical extent of observed dust extinction and can exceed 8 km. This was confirmed by Teixeira et al. (2016) in their sensitivity study to the vertical resolution during a Saharan dust event. When comparing model results to the observed vertical profiles, they showed that in all different configurations, the model broadly reproduced the features of the observed extinction coefficient profile by CALIOP.

This study also highlighted the need to use different data sources to better assess the model vertical profile because by using CALIPSO only, there are often missing data in areas where important processes are responsible for dust emissions and its distribution in the atmosphere. Between the three emission schemes, the simulated extinction profiles indicate that the locations of dust are largely consistent. The GOCART and AFWA schemes show the largest areas in extent of extinction coefficient than the UoC scheme. The amount of simulated dust extinction coefficient profiles in the atmosphere is higher than the amount

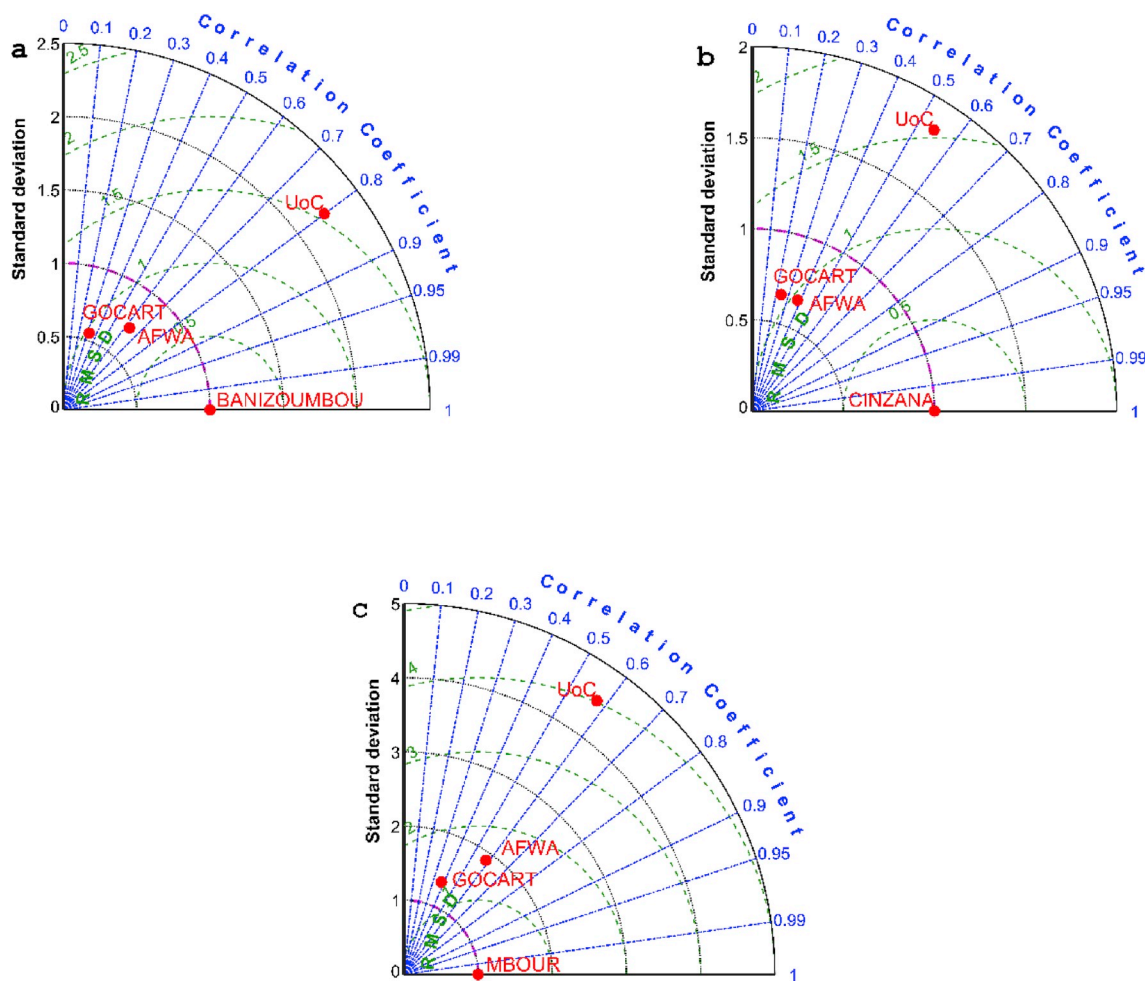


Fig. 6. Taylor diagram comparing dust AOD values over June-July-August 2006, from AERONET observations, a) Banizoumbou, b) Cinzana, c) M'bour at 550 nm, and simulated by the Weather Research and Forecasting model coupled with chemistry (WRF-Chem) from, the Goddard Global Ozone Chemistry Aerosol Radiation and Transport (GOCART) scheme, the Air Force Weather Agency (AFWA) scheme and the University of Cologne (UoC) scheme.

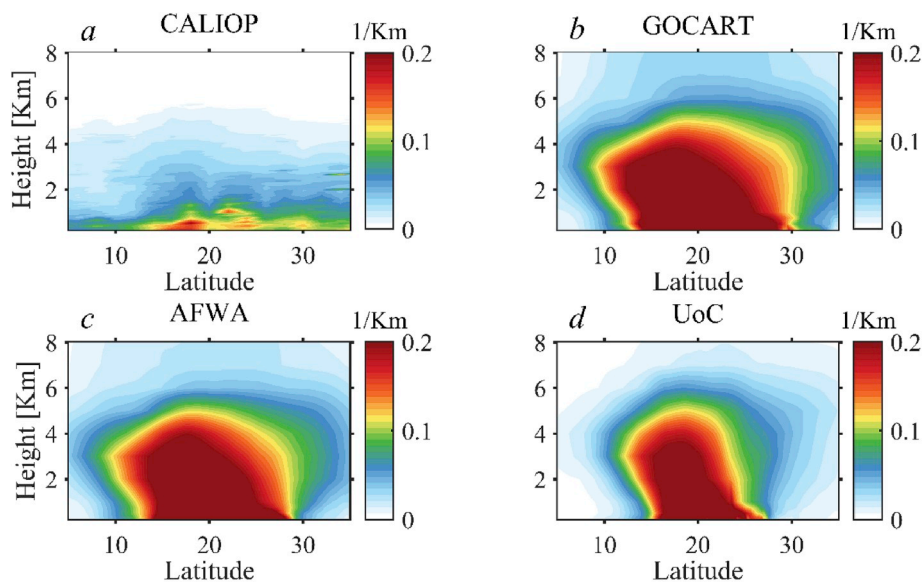


Fig. 7. Dust extinction coefficient (1/km) vertical profile averaged over the longitude (20 W, 35 E) over June-July-August 2006, from the CALIOP at 532 nm, and the simulated at 550 nm, by the Weather Research and Forecasting model coupled with chemistry (WRF-Chem), from the Goddard Global Ozone Chemistry Aerosol Radiation and Transport (GOCART) scheme, the Air Force Weather Agency (AFWA) scheme, and the University of Cologne (UoC) scheme.

observed by the CALIOP. The three dust emission schemes show similar distribution as CALIOP but overestimate broadly the maximums and vertical extent. This may be due to the fact that wet deposition is not included in the simulations which could reduce the extent and magnitude of simulated dust.

4. Conclusions

The objective of this study was to compare the simulated dust AOD and extinction coefficient from different dust emission schemes within the WRF-Chem model over the northern Africa region. The performance of each dust emission scheme to replicate the observation was assessed by CALIPSO and AERONET ground-based observations during the summer of 2006 over northern Africa. The three schemes showed their capability to reproduce broadly the dust source regions, the dust AOD and extinction profile observed by the CALIOP and AERONET ground-based over northern Africa. All three schemes produce a large amount of dust content compared to the observation made by CALIOP. None of the three schemes performs very well in capturing the spatial distribution pattern and magnitude by CALIOP observation. The GOCART and AFWA schemes produce similar patterns of AOD in terms of extent while the UoC scheme produces localized AOD over the Sahel region. The three schemes show similar daily variation compared to observations made by the AERONET stations but certain peaks are simulated slightly in advance or delay to observations.

In Banizoumbou station, the AFWA and UoC schemes perform better in terms of high correlation values compared to the GOCART scheme. In Cinzana station, the UoC scheme performs better in terms of correlation and normalized bias but has a large percentage of normalized root mean square error compared to the other two schemes (GOCART and AFWA). The AFWA scheme is much closer to the observation in terms of intensity in both Banizoumbou and Cinzana stations. In M'Bour station, the AFWA and UoC schemes are well correlated than the GOCART scheme but in terms of the intensity, the GOCART scheme is closer to the observation and has a lower normalized root mean square error.

The dust extinction coefficient vertical profiles observed from the three schemes generally agreed with the one retrieved from CALIOP. The highest extinction coefficient values from CALIOP were found in the lower levels of the atmosphere below 1 km due to the amount of desert dust in the region. On the other hand, all the three schemes (GOCART,

AFWA, and UoC) overestimate broadly the dust extinction coefficient profiles observed by CALIOP in terms of vertical extent and magnitude over northern Africa. Our results highlight significant differences between the three schemes. These differences could be related to the calculation of the threshold wind speed in each scheme. Furthermore, the indirect effects of dust and wet deposition were not considered and this could also affect the simulated results in reproducing the observation. Our results highlight as well the need to better-improving dust emission parameterizations in the WRF-Chem model because uncertainties still exist in reproducing correctly the atmospheric dust load.

This study presents an evaluation of dust emission schemes into the WRF-Chem model over northern Africa. However, further studies are necessary to understand the complexity of the mechanisms of dust emissions, transport and their climatic effect in North Africa.

Funding

This study is supported by the National Natural Science Foundation of China grants (41675004&41975002).

Data availability

Data will be provided and made available upon the request of the readers.

Declaration of competing interest

Authors declare no conflict of interest in the present work.

Acknowledgments

We acknowledge the NOAA/NCEP, NOAA/ESRL and NCAR for their WRF-Chem model, which was used in this study. The author is thankful to the Government of the Republic of Niger, the China Scholarship Council (CSC) and Nanjing University of Information Science and Technology (NUIST) for providing the needed resources. CALIPSO data were obtained from the NASA Langley Research Center Atmospheric Sciences Data Center.

References

- Adams, A.M., Prospero, J.M., Zhang, C., 2012. CALIPSO-derived three-dimensional structure of aerosol over the Atlantic Basin and adjacent continents. *J. Clim.* 25, 6862–6879.
- Allen, R.J., Amiri-Farahani, A., Lamarque, J.-F., Smith, C., Shindell, D., Hassan, T., Chung, C.E., 2019. Observationally constrained aerosol–cloud semi-direct effects. *npj Climate and Atmospheric Science* 2. <https://doi.org/10.1038/s41612-019-0073-9>.
- Alpert, P., Krichak, S.O., Tsidulko, M., Shafir, H., Joseph, J.H., 2002. A dust prediction system with TOMS initialization. *Mon. Weather Rev.* 130, 2335–2345. [https://doi.org/10.1175/1520-0493\(2002\)130<2335:ADPSWT>2.0.CO;2](https://doi.org/10.1175/1520-0493(2002)130<2335:ADPSWT>2.0.CO;2).
- Amiri-Farahani, A., Allen, R., Li, K., Chu, J., 2019. The semi-direct effect of combined dust and sea salt aerosols in a multi-model analysis. *Geophys. Res. Lett.* <https://doi.org/10.1029/2019GL084590>.
- Amiri-Farahani, A., Allen, R.J., Neubauer, D., Lohmann, U., 2017. Impact of Saharan dust on North Atlantic marine stratocumulus clouds: importance of the semidirect effect. *Atmos. Chem. Phys.* 17, 6305–6322. <https://doi.org/10.5194/acp-17-6305-2017>.
- Bagnold, R.A., 1941. *The Physics of Blown Sand and Desert Dunes*. Methuen, London, 1941.
- Barkan, J., Kutiel, H., Alpert, P., 2004. Climatology of dust sources in north Africa and the arabian peninsula, based on TOMS data. *Indoor Built Environ.* 13, 407–419.
- Barnard, J.C., Fast, J.D., Paredes-Miranda, G., Arnott, W.P., Laskin, A., 2010. Evaluation of the WRF-chem² aerosol chemical to aerosol optical properties² module using data from the MILAGRO campaign. *Atmos. Chem. Phys.* 10, 7325–7340.
- Beljaars, A.C., 1995. The parametrization of surface fluxes in large-scale models under free convection. *Q. J. R. Meteorol. Soc.* 121, 255–270.
- Briant, R., Tuccella, P., Deroubaix, A., Khvorostyanov, D., Menut, L., Mailler, S., Turquet, S., 2017. Aerosol–radiation interaction modelling using online coupling between the WRF 3.7.1 meteorological model and the CHIMERE 2016 chemistry-transport model, through the OASIS3-MCT coupler. *Geosci. Model Dev. (GMD)* 10, 927–944. <https://doi.org/10.5194/gmd-10-927-2017>.
- Chapman, E.G., Gustafson Jr., W.I., Easter, R.C., Barnard, J.C., Ghan, S.J., Pekour, M.S., Fast, J.D., 2009. Coupling aerosol-cloud-radiative processes in the WRF-Chem model: investigating the radiative impact of elevated point sources. *Atmos. Chem. Phys.* 9, 945–964.
- Defries, R.S., Townshend, J.R.G., 1999. Global land cover characterization from satellite data: from research to operational implementation? *Global Ecol. Biogeogr.* 8, 367–379. <https://doi.org/10.1046/j.1365-2699.1999.00139.x>.
- Dyer, A.J., Hicks, B.B., 1970. Flux-gradient relationships in the constant flux layer. *Q. J. R. Meteorol. Soc.* 96, 715–721.
- Eltahan, M., Shokr, M., Sherif, A., 2018. Simulation of severe dust events over Egypt using tuned dust schemes in weather research forecast (WRF-Chem). *Atmosphere* 9, 246.
- Engelstaedter, S., Tegen, I., Washington, R., 2006. North African dust emissions and transport. *Earth Sci. Rev.* 79, 73–100.
- Evan, A.T., Fiedler, S., Zhao, C., Menut, L., Schepanski, K., Flamant, C., Doherty, O., 2015. Derivation of an observation-based map of North African dust emission. *Aeolian Research* 16, 153–162. <https://doi.org/10.1016/j.aeolia.2015.01.001>.
- Evan, A.T., Flamant, C., Gaetani, M., Guichard, F., 2016. The past, present and future of African dust. *Nature* 531, 493–495. <https://doi.org/10.1038/nature17149>.
- Fast, J.D., Gustafson Jr., W.I., Easter, R.C., Zaveri, R.A., Barnard, J.C., Chapman, E.G., Grell, G.A., Peckham, S.E., 2006. Evolution of ozone, particulates, and aerosol direct radiative forcing in the vicinity of Houston using a fully coupled meteorology-chemistry-aerosol model. *J. Geophys. Res.: Atmosphere* 111. <https://doi.org/10.1029/2005JD006721>.
- Fiedler, S., Schepanski, K., Heinold, B., Knippertz, P., Tegen, I., 2013. Climatology of nocturnal low-level jets over North Africa and implications for modeling mineral dust emission: nocturnal low-level jet climatology. *J. Geophys. Res.: Atmosphere* 118, 6100–6121. <https://doi.org/10.1002/jgrd.50394>.
- Fiedler, S., Schepanski, K., Knippertz, P., Heinold, B., Tegen, I., 2014. How important are atmospheric depressions and mobile cyclones for emitting mineral dust aerosol in North Africa? *Atmos. Chem. Phys.* 14, 8983–9000.
- Flaounas, E., Kotroni, V., Lagouvardos, K., Klose, M., Flamant, C., Giannaros, T.M., 2017. Sensitivity of the WRF-Chem (V3. 6.1) model to different dust emission parametrisation: assessment in the broader Mediterranean region. *Geosci. Model Dev. (GMD)* 10, 2925–2945.
- García, O.E., Díaz, J.P., Expósito, F.J., Díaz, A.M., Dubovik, O., Dubuisson, P., Roger, J.-C., 2012. Shortwave radiative forcing and efficiency of key aerosol types using AERONET data. *Atmos. Chem. Phys.* 12, 5129.
- Gillett, D.A., 1979. Environmental factors affecting dust emission by wind erosion. *Saharan dust* 71–94.
- Gillette, D.A., 1981. Production of dust that may be carried great distances. *Geological Society of America Special Papers*. Geological Society of America, pp. 11–26. <https://doi.org/10.1130/SPE186-p11>.
- Gillette, D.A., Passi, R., 1988. Modeling dust emission caused by wind erosion. *J. Geophys. Res.: Atmosphere* 93, 14233–14242.
- Genoux, P., Chin, M., Tegen, I., Prospero, J.M., Holben, B., Dubovik, O., Lin, S.-J., 2001. Sources and distributions of dust aerosols simulated with the GOCART model. *J. Geophys. Res.: Atmosphere* 106, 20255–20273.
- Genoux, P., Prospero, J.M., Torres, O., Chin, M., 2004. Long-term simulation of global dust distribution with the GOCART model: correlation with North Atlantic Oscillation. *Environ. Model. Software* 19, 113–128.
- Goudie, A.S., Middleton, N.J., 2001. Saharan dust storms: nature and consequences. *Earth Sci. Rev.* 56, 179–204.
- Graaf, M. de, Tilstra, L.G., Stammes, P., 2019. Aerosol direct radiative effect over clouds from a synergy of ozone monitoring instrument (OMI) and moderate resolution imaging spectroradiometer (MODIS) reflectances. *Atmospheric Measurement Techniques* 12, 5119–5135. <https://doi.org/10.5194/amt-12-5119-2019>.
- Grell, G.A., 1993. Prognostic evaluation of assumptions used by cumulus parameterizations. *Mon. Weather Rev.* 121, 764–787.
- Grell, G.A., Dévényi, D., 2002. A generalized approach to parameterizing convection combining ensemble and data assimilation techniques. *Geophys. Res. Lett.* 29, 38–41. <https://doi.org/10.1029/2002GL015311>.
- Grell, G.A., Peckham, S.E., Schmitz, R., McKeen, S.A., Frost, G., Skamarock, W.C., Eder, B., 2005. Fully coupled “online” chemistry within the WRF model. *Atmos. Environ.* 39, 6957–6975.
- Gu, Y., Liou, K.N., Jiang, J.H., Su, H., Liu, X., 2012. Dust aerosol impact on North Africa climate: a GCM investigation of aerosol-cloud-radiation interactions using A-Train satellite data. *Atmos. Chem. Phys.* 12, 1667–1679.
- Haustein, K., Washington, R., King, J., Wiggs, G., Thomas, D.S.G., Eckardt, F.D., Bryant, R.G., Menut, L., 2015. Testing the performance of state-of-the-art dust emission schemes using DO4Models field data. *Geosci. Model Dev. (GMD)* 8, 341.
- Haywood, J., Boucher, O., 2000. Estimates of the direct and indirect radiative forcing due to tropospheric aerosols: a review. *Rev. Geophys.* 38, 513–543. <https://doi.org/10.1029/1999RG000078>.
- Heald, C.L., Ridley, D.A., Kroll, J.H., Barrett, S.R.H., Cady-Pereira, K.E., Alvarado, M.J., Holmes, C.D., 2014. Contrasting the direct radiative effect and direct radiative forcing of aerosols. *Atmos. Chem. Phys.* 14, 5513–5527.
- Hoff, R.M., Christopher, S.A., 2009. Remote sensing of particulate pollution from space: have we reached the promised land? *J. Air Waste Manag. Assoc.* 59, 645–675.
- Holben, B.N., Eck, T.F., Slutsker, I., Tanre, D., Buis, J.P., Setzer, A., Vermote, E., Reagan, J.A., Kaufman, Y.J., Nakajima, T., 1998. AERONET—a federated instrument network and data archive for aerosol characterization. *Remote Sens. Environ.* 66, 1–16.
- Hong, S.-Y., Noh, Y., Dudhia, J., 2006. A new vertical diffusion package with an explicit treatment of entrainment processes. *Mon. Weather Rev.* 134, 2318–2341.
- Iacono, M.J., Delamere, J.S., Mlawer, E.J., Shephard, M.W., Clough, S.A., Collins, W.D., 2008. Radiative forcing by long-lived greenhouse gases: calculations with the AER radiative transfer models. *J. Geophys. Res.: Atmosphere* 113.
- Jones, C., Mahowald, N., Luo, C., 2003. The role of easterly waves on African desert dust transport. *J. Clim.* 16, 3617–3628.
- Jones, S.L., Adams-Selin, R., Hunt, E.D., Creighton, G.A., Cetola, J.D., 2012. Update on modifications to WRF-CHEM GOCART for fine-scale dust forecasting at AFWA. AGU Fall Meeting Abstracts.
- Kalashnikova, O.V., Sokolik, I.N., 2002. Importance of shapes and compositions of wind-blown dust particles for remote sensing at solar wavelengths. *Geophys. Res. Lett.* 29, 38–41. <https://doi.org/10.1029/2002GL014947>.
- Kawamura, R., 1951. Study on sand movement by wind (Relationship between sand flow and wind friction, and vertical density distribution of sand). 5. Tokyo Daigaku Rikogaku Kenkyusho Hokoku, Tokyo, pp. 95–112.
- Kim, S.-W., Chazette, P., Dulac, F., Sanak, J., Johnson, B., Yoon, S.-C., 2009. Vertical structure of aerosols and water vapor over West Africa during the African monsoon dry season. *Atmos. Chem. Phys.* 9.
- Knippertz, P., Todd, M.C., 2010. The central west Saharan dust hot spot and its relation to African easterly waves and extratropical disturbances. *J. Geophys. Res.: Atmosphere* 115.
- Koch, D., Del Genio, A.D., 2010. Black carbon semi-direct effects on cloud cover: review and synthesis. *Atmos. Chem. Phys.* 10, 7685–7696.
- Kok, J.F., 2011. A scaling theory for the size distribution of emitted dust aerosols suggests climate models underestimate the size of the global dust cycle. *Proc. Natl. Acad. Sci. Unit. States Am.* 108, 1016–1021. <https://doi.org/10.1073/pnas.1014798108>.
- Kok, J.F., Parteli, E.J.R., Michaels, T.I., Karam, D.B., 2012. The physics of wind-blown sand and dust. *Rep. Prog. Phys.* 75, 106901. <https://doi.org/10.1088/0034-4885/75/10/106901>.
- Kok, J.F., Ridley, D.A., Zhou, Q., Miller, R.L., Zhao, C., Heald, C.L., Ward, D.S., Albani, S., Haustein, K., 2017. Smaller desert dust cooling effect estimated from analysis of dust size and abundance. *Nat. Geosci.* 10, 274–278. <https://doi.org/10.1038/ngeo2912>.
- Kokkalis, P., K Al Jassar, H., Solomos, S., Raptis, P.-I., Al Hendi, H., Amiridis, V., Papayannis, A., Al Sarraf, H., Al Dimashki, M., 2018. Long-Term ground-based measurements of aerosol optical depth over Kuwait city. *Rem. Sens.* 10, 1807.
- LeGrand, S.L., Polashenski, C., Letcher, T.W., Creighton, G.A., Peckham, S.E., Cetola, J.D., 2019. The AFWA dust emission scheme for the GOCART aerosol model in WRF-Chem v3. 8.1, 12. Geoscientific Model Development, pp. 131–166.
- Lin, Y.-L., Farley, R.D., Orville, H.D., 1983. Bulk parameterization of the snow field in a cloud model. *J. Clim. Appl. Meteorol.* 22, 1065–1092.
- Lohmann, U., Feichter, J., 2005. Global indirect aerosol effects: a review. *Atmos. Chem. Phys.* 5, 715–737.
- Ma, X., Bartlett, K., Harmon, K., Yu, F., 2013. Comparison of AOD between CALIPSO and MODIS: significant differences over major dust and biomass burning regions. *Atmospheric Measurement Techniques* 6, 2391–2401.
- Ma, X., Yu, F., Luo, G., 2012. Aerosol direct radiative forcing based on GEOS-Chem-APM and uncertainties. *Atmos. Chem. Phys.* 12, 5563–5581.
- Marticorena, B., Bergametti, G., 1995. Modeling the atmospheric dust cycle: 1. Design of a soil-derived dust emission scheme. *J. Geophys. Res.: Atmosphere* 100, 16415–16430.
- Marticorena, B., Chatenet, B., Rajot, J.-L., Bergametti, G., Deroubaix, A., Vincent, J., Kouli, A., Schmechtig, C., Coulibaly, M., Diallo, A., 2017. Mineral dust over west and central Sahel: seasonal patterns of dry and wet deposition fluxes from a pluriannual sampling (2006–2012). *J. Geophys. Res.: Atmosphere* 122, 1338–1364.

- Marticoarena, B., Chatenet, B., Rajot, J.-L., Traoré, S., Coulibaly, M., Diallo, A., Koné, I., Maman, A., NDiaye, T., Zakou, A., 2010. Temporal variability of mineral dust concentrations over West Africa: analyses of a pluriannual monitoring from the AMMA Sahelian Dust Transect. *Atmos. Chem. Phys.* 10, 8899–8915.
- Menut, L., Pérez, C., Haustein, K., Bessagnet, B., Prigent, C., Alfaro, S., 2013. Impact of surface roughness and soil texture on mineral dust emission fluxes modeling: impact of roughness and soil texture on mineral dust. *J. Geophys. Res.: Atmosphere* 118, 6505–6520. <https://doi.org/10.1002/jgrd.50313>.
- Miller, R.L., Periwit, J., Tegen, I., 2004. Feedback upon dust emission by dust radiative forcing through the planetary boundary layer. *J. Geophys. Res.: Atmosphere* 109. <https://doi.org/10.1029/2004JD004912>.
- Mukul Tewari, N., Tewari, M., Chen, F., Wang, W., Dudhia, J., LeMone, M.A., Mitchell, K., Ek, M., Gayno, G., Wegiel, J., 2004. Implementation and verification of the unified NOAA land surface model in the WRF model. 20th Conference on Weather Analysis and Forecasting/16th Conference on Numerical Weather Prediction, pp. 11–15. Formerly Paper Number 17.5).
- Nabat, P., Somot, S., Mallet, M., Sevault, F., Chiacchio, M., Wild, M., 2015. Direct and semi-direct aerosol radiative effect on the Mediterranean climate variability using a coupled regional climate system model. *Clim. Dynam.* 44, 1127–1155.
- Nicholson, S., 2000. Land surface processes and Sahel climate. *Rev. Geophys.* 38, 117–139.
- Otto, S., Reus, M. de, Trautmann, T., Thomas, A., Wendisch, M., Borrmann, S., 2007. Atmospheric radiative effects of an in situ measured Saharan dust plume and the role of large particles. *Atmos. Chem. Phys.* 7, 4887–4903.
- Paulson, C.A., 1970. The mathematical representation of wind speed and temperature profiles in the unstable atmospheric surface layer. *J. Appl. Meteorol.* 9, 857–861.
- Péré, J.C., Mallet, M., Pont, V., Bessagnet, B., 2011. Impact of aerosol direct radiative forcing on the radiative budget, surface heat fluxes, and atmospheric dynamics during the heat wave of summer 2003 over western Europe: a modeling study: aerosol direct radiative impacts. *J. Geophys. Res.: Atmosphere* 116, n/a–n/a. <https://doi.org/10.1029/2011JD016240>.
- Powell, K.A., Hostetler, C.A., Vaughan, M.A., Lee, K.-P., Trepte, C.R., Rogers, R.R., Winker, D.M., Liu, Z., Kuehn, R.E., Hunt, W.H., 2009. CALIPSO lidar calibration algorithms. Part I: nighttime 532-nm parallel channel and 532-nm perpendicular channel. *J. Atmos. Ocean. Technol.* 26, 2015–2033.
- Prospero, J.M., 1996. Saharan dust transport over the north Atlantic Ocean and Mediterranean: an overview. *The Impact of Desert Dust across the Mediterranean*. Springer, pp. 133–151.
- Prospero, J.M., Ginoux, P., Torres, O., Nicholson, S.E., Gill, T.E., 2002. Environmental characterization of global sources of atmospheric soil dust identified with the Nimbus 7 Total Ozone Mapping Spectrometer (TOMS) absorbing aerosol product. *Rev. Geophys.* 40.
- Prospero, J.M., Mayol-Bracero, O.L., 2013. Understanding the transport and impact of african dust on the caribbean basin. *Bull. Am. Meteorol. Soc.* 94, 1329–1337. <https://doi.org/10.1175/BAMS-D-12-00142.1>.
- Quijano, A.L., Sokolik, I.N., Toon, O.B., 2000. Radiative heating rates and direct radiative forcing by mineral dust in cloudy atmospheric conditions. *J. Geophys. Res.: Atmosphere* 105, 12207–12219.
- Scanza, R.A., Mahowald, N., Ghan, S., Zender, C.S., Kok, J.F., Liu, X., Zhang, Y., Albani, S., 2015. Modeling dust as component minerals in the Community Atmosphere Model: development of framework and impact on radiative forcing. *Atmos. Chem. Phys.* 15, 537–561. <https://doi.org/10.5194/acp-15-537-2015>.
- Schläditz, A., Müller, T., Kaaden, N., Massling, A., Kandler, K., Ebert, M., Weinbruch, S., Deutscher, C., Wiedensohler, A., 2009. In situ measurements of optical properties at tinou (Morocco) during the saharan mineral dust experiment SAMUM 2006. *Tellus Ser. B Chem. Phys. Meteorol.* B 61, 64–78. <https://doi.org/10.1111/j.1600-0889.2008.00397.x>.
- Schmechtig, C., Marticoarena, B., Chatenet, B., Bergametti, G., Rajot, J.L., Coman, A., 2011. Simulation of the mineral dust content over Western Africa from the event to the annual scale with the CHIMERE-DUST model. *Atmos. Chem. Phys.* 11, 7185–7207. <https://doi.org/10.5194/acp-11-7185-2011>.
- Sekiguchi, M., Nakajima, T., Suzuki, K., Kawamoto, K., Higurashi, A., Rosenfeld, D., Sano, I., Mukai, S., 2003. A study of the direct and indirect effects of aerosols using global satellite data sets of aerosol and cloud parameters. *J. Geophys. Res.: Atmosphere* 108. <https://doi.org/10.1029/2002JD003359>.
- Shao, Y., 2001. A model for mineral dust emission. *J. Geophys. Res.: Atmosphere* 106, 20239–20254. <https://doi.org/10.1029/2001JD900171>.
- Shao, Y., 2004. Simplification of a dust emission scheme and comparison with data. *J. Geophys. Res.: Atmosphere* 109.
- Shao, Y., Ishizuka, M., Mikami, M., Leys, J.F., 2011. Parameterization of size-resolved dust emission and validation with measurements. *J. Geophys. Res.: Atmosphere* 116.
- Slingo, A., Ackerman, T.P., Allan, R.P., Kassianov, E.I., McFarlane, S.A., Robinson, G.J., Barnard, J.C., Miller, M.A., Harries, J.E., Russell, J.E., 2006. Observations of the impact of a major Saharan dust storm on the atmospheric radiation balance. *Geophys. Res. Lett.* 33.
- Slingo, A., Bharmal, N.A., Robinson, G.J., Settle, J.J., Allan, R.P., White, H.E., Lamb, P.J., Lele, M.I., Turner, D.D., McFarlane, S., 2008. Overview of observations from the RADAGAST experiment in Niamey, Niger: meteorology and thermodynamic variables. *J. Geophys. Res.: Atmosphere* 113.
- Solmon, F., Mallet, M., Elguindi, N., Giorgi, F., Zakey, A., Konaré, A., 2008. Dust aerosol impact on regional precipitation over western Africa, mechanisms and sensitivity to absorption properties. *Geophys. Res. Lett.* 35.
- Teixeira, J.C., Carvalho, A.C., Tuccella, P., Curci, G., Rocha, A., 2016. WRF-chem sensitivity to vertical resolution during a saharan dust event. *Phys. Chem. Earth, Parts A/B/C* 94, 188–195.
- Twomey, S., 1977. The influence of pollution on the shortwave albedo of clouds. *J. Atmos. Sci.* 34, 1149–1152.
- Voss, K.K., Evan, A.T., 2019. A new satellite-based global climatology of dust aerosol optical depth. *J. Appl. Meteor. Climatol.* <https://doi.org/10.1175/JAMC-D-19-0194.1>.
- Webb, E.K., 1970. Profile relationships: the log-linear range, and extension to strong stability. *Q. J. R. Meteorol. Soc.* 96, 67–90.
- Wesely, M.L., 1989. Parameterization of surface resistances to gaseous dry deposition in regional-scale numerical models. *Atmos. Environ.* 23, 1293–1304, 1967.
- Winker, D.M., Hunt, W.H., Hostetler, C.A., 2004. Status and performance of the CALIOP lidar. *Laser Radar Techniques for Atmospheric Sensing*. International Society for Optics and Photonics, pp. 8–16.
- Winker, D.M., Hunt, W.H., McGill, M.J., 2007. Initial performance assessment of CALIOP. *Geophys. Res. Lett.* 34.
- Winker, D.M., Tackett, J.L., Getzewich, B.J., Liu, Z., Vaughan, M.A., Rogers, R.R., 2013. The global 3-D distribution of tropospheric aerosols as characterized by CALIOP. *Atmos. Chem. Phys.* 13, 3345–3361.
- Yahi, H., Marticoarena, B., Thiria, S., Chatenet, B., Schmechtig, C., Rajot, J.L., Crepon, M., 2013. Statistical relationship between surface PM₁₀ concentration and aerosol optical depth over the Sahel as a function of weather type, using neural network methodology: weather types and mineral dust content. *J. Geophys. Res.: Atmosphere* 118 (13), 265–313. <https://doi.org/10.1002/2013JD019465>, 281.
- Zhang, D., Anthes, R.A., 1982. A high-resolution model of the planetary boundary layer—sensitivity tests and comparisons with SESAME-79 data. *J. Appl. Meteorol.* 21, 1594–1609.